IEEE Access
Multidisciplinary | Rapid Review | Open Access Journal

Received 29 July 2023, accepted 8 August 2023, date of publication 17 August 2023, date of current version 23 August 2023.

Digital Object Identifier 10.1109/ACCESS.2023.3305994

RESEARCH ARTICLE

Generating Chest X-Ray Progression of Pneumonia Using Conditional Cycle Generative Adversarial Networks

YEONGBONG JIN[1], WOOJIN CHANG[1], AND BONGGYUN KO[2,3]
[1]Department of Industrial Engineering, Seoul National University, Seoul 08826, South Korea
[2]Department of Mathematics and Statistics, Chonnam National University, Gwangju 61186, South Korea
[3]Research and Development Center, XRAI Inc., Gwangju 61186, South Korea

Corresponding author: Bonggyun Ko (bonggyun.ko@jnu.ac.kr)

This work was supported in part by the National Research Foundation of Korea (NRF) Grant funded by the Korea Government through MSIT under Grant 2019R1G1A1100704, Grant 2021R1F1A1060049, and Grant 2022M3A9E4017151; in part by the Chonnam National University under Grant 2020-2010; and in part by the BK21 Fostering Outstanding Universities for Research (FOUR) funded by the Ministry of Education (MOE), South Korea, and the National Research Foundation of Korea (NRF), under Grant 5120200913674.

ABSTRACT Pneumonia is an inflammation of the lungs caused by pathogens or autoimmune diseases, with about 450 million patients worldwide each year. Chest X–ray analysis is the most common radiographic method used to diagnose pneumonia, and advances in deep learning have led to the availability of high-dimensional image, audio, and video data. Deep learning is being applied in many fields, including the medical field, where numerous researchers have attempted to use it for computer-aided diagnosis. Recently, with the appearance of generative adversarial networks, it is possible to generate plausible and realistic images. In this paper, we combined cycle Generative Adversarial Networks (GANs) and conditional GANs, which are extensions of GANs, to convert the domains between images and generate images of the intermediate domains. We conducted the domain change between pneumonia images and normal images by applying our framework to a Chest X–ray image dataset. We evaluated the domain change by redefining the ResNet152-based classifier, and we generated the pneumonia progression images by inputting a value between two domains in the conditional vector of the generator. We then evaluated the ability of the trained GANs by comparing the original dataset with the generated dataset, and generated plausible progression images of pneumonia.

INDEX TERMS Chest X–ray, generative adversarial networks, pneumonia, transfer learning.

I. INTRODUCTION

Pneumonia is a respiratory infection that affects the lungs and is a common illness. It is usually caused by bacteria, viruses, or fungi, although other microorganisms can also cause it. Pneumonia spreads by direct contact with an infected person. Approximately 450 million people worldwide suffer from pneumonia each year, and it results in about 4 million deaths annually [1]. In particular, there is a greater risk of death for children under 5 years of age [1]; in 2015, there were 5.9 million deaths from pneumonia among children under age 5 [2]. These large numbers of patients serve as evidence that efforts are needed to prevent and overcome pneumonia, but the emergence of severe acute respiratory syndrome, Middle East respiratory syndrome, COVID–19, and other diseases has highlighted the importance of countermeasures related to acute viral pneumonia. To date, the chest X-ray (CXR) has been the most common radiographic method for diagnosing pneumonia [3], and a number of researchers have studied using CXR for disease detection and prediction using deep learning [4], [5], [6], [7], [8].

Deep learning algorithms have improved with impressive performance in computer vision [9], [10], [11], speech recognition [12], natural language processing [13], and many

The associate editor coordinating the review of this manuscript and approving it for publication was Santosh Kumar.

other tasks such as recommendation systems [14], [15] and medical field [16], [17]. This development of deep learning methods attracted attention by showing high accuracy and performance in computer–aided diagnosis and medical image analysis [18], [19], [20]. Through supervised learning, many works aimed to identify the boundary of diseases. However, with the advent of generative adversarial networks (GANs), the focus shifted to generative models and distribution learning.

GANs are neural network structures that consist of generator G and discriminator D [21]. G produces fake data points from a latent vector, and D distinguishes between real data and fake data. Through this series of adversarial learning, G and D develop each other's abilities, and G can generate images that D cannot distinguish.

The GANs, proposed by Goodfellow et al. [21] in 2014, induced great interest due to their ability to generate realistic data points. In the medical imaging field, it was demonstrated to boost performance [7], [8]. GANs can be used to overcome the limitation of medical image analysis that it is not possible to delineate disease severity by allowing for data augmentation or for generating previously unseen images [22], [23].

In this paper, we propose the method of visualizing the progression of pneumonia through conversion between normal and pneumonia CXR images using CycleGANs [24], which is a kind of GANs; we present the conditional CycleGANs that we used in Fig. 1. Previously, it was difficult for patients to identify the disease even looking at their CXRs; however, we expect that our method will allow patients to visually confirm the progress of the disease on CXR, which will increase their cooperation with effort to treat them. In addition, from the medical point of view, it may be possible to build a clinical algorithm using CXR through analysis to identify where the GANs determine that there is pneumonia.

We suggest the following contributions of our work:

1) We propose a method for maximizing visual comprehension by showing how CXR images change from normal with the progression of pneumonia (or vice versa), which can be used as a motivation for treatment. Patients with pneumonia can view their X-ray images and confirm for themselves that they have the disease.
2) We were able to generate high-resolution images (256×256) because the CycleGANs increased stability by using original GANs loss and L_1 loss together.
3) CXR images generated throughout the disease progression can increase visual understanding of a pneumonia diagnosis, and we expect that the technique can apply to other progressive processes.

The remainder of this paper is summarized as follows: In Section II, we explain the background related to our works, including the application of deep learning in medical imaging, the GANs, and their variations. We describe the datasets and methodologies used in our experiment in Section III, and in Sections IV and V, we present the experimental results and our evaluations of the findings.

II. RELATED WORK

The GANs can learn the distribution of a given dataset and generate fake samples through an adversarial process [21]. The loss function of general GANs is defined as:

$$\mathcal{L}_{\text{GANs}}(G, D) = \min_{G} \max_{D} \{\mathbb{E}_{x\sim p_{data}(x)}[\log D(x)] + \mathbb{E}_{z\sim p_z(z)}[\log(1 - D(G(z)))]\} \quad (1)$$

The generator G takes random noise z from distribution $p_z(z)$ as input and generates fake samples, and the distribution of generated data is learned to follow the real data distribution $p_{data}(x)$; in contrast, the discriminator D learns to distinguish between fake data and real data. Since the introduction of the GANs, there have been many variations through follow-up research.

Conditional GANs (cGANs) [25], one of the GANs extensions, are structures that are transformed into a conditional form by adding an information vector c to the GANs structure. This makes it possible to generate images with specific properties (conditions). When c is additionally input as conditional information, the cGANs loss function used in this study is defined as:

$$\mathcal{L}_{\text{cGANs}}(G, D) = \min_{G} \max_{D} \{\mathbb{E}_{x\sim p_{data}(x)}[(D(x) - 1)^2] + \mathbb{E}_{x\sim p_x(x)}[(D(G(x \mid c)))^2]\} \quad (2)$$

CycleGANs [24] are useful tools for image–to–image translation with unpaired data. The method learns when two different domains, original domain X and target domain Y, are given using the GANs structure, so that each can be converted to the other's style. CycleGANs are composed of four neural networks, two generators and two discriminators. The first generator, $G_{X\to Y}$, converts the images of domain X to Y, and the second generator, $G_{Y\to X}$, converts the domain Y images to X. D_X and D_Y are discriminators for domain X and domain Y, respectively. D_X is trained to distinguish between the real images in domain X and the fake images generated by generator $G_{Y\to X}$ and similarly, D_Y is trained to distinguish between the real images in domain Y and the fake images generated by generator $G_{X\to Y}$. CycleGANs solve the problem of unpaired training data by introducing Cycle Consistency, and Cycle Consistency means that an image can produce a corresponding pair of images by going through one cycle of the generators. The full loss function of CycleGANs, including Cycle Consistency, follows as:

$$\mathcal{L}(G_{X\to Y}, G_{Y\to X}, D_X, D_Y) = \mathcal{L}_{\text{GANs}}(G_{X\to Y}, D_Y) + \mathcal{L}_{\text{GANs}}(G_{Y\to X}, D_X) + \lambda\mathcal{L}_{\text{CYC}}(G_{X\to Y}, G_{Y\to X}) \quad (3)$$

where λ is the hyper–parameter that controls the weight of the Cycle Consistency which is defined follows as:

$$\mathcal{L}_{\text{CYC}}(G_{X\to Y}, G_{Y\to X}) = \| G_{Y\to X}(G_{X\to Y}(x)) - x \|_1 + \| G_{X\to Y}(G_{Y\to X}(y)) - y \|_1 \quad (4)$$

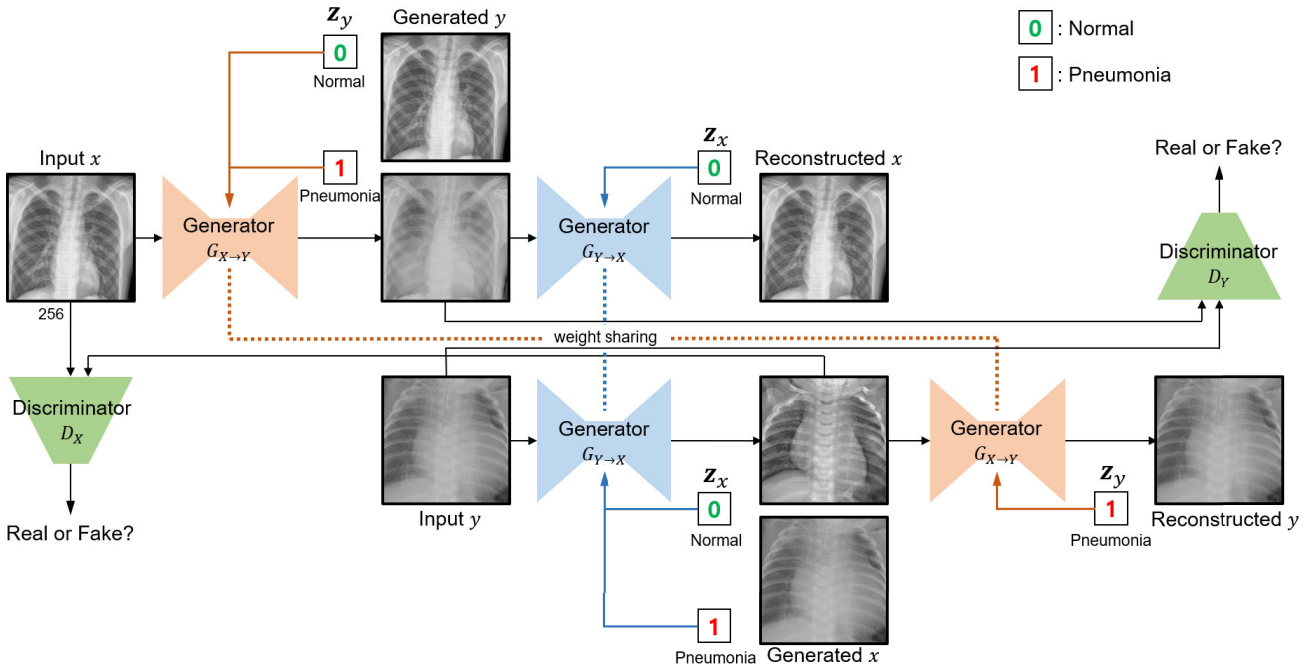

FIGURE 1. The overall framework for generating chest X–ray progression of pneumonia.

In addition, there has been much research on applying GANs and improving its performance of the GANs. In this paper, the GANs structures we addressed were the cGANs and CycleGANs for changing styles to obtain the desired image. Specifically, we used conditional CycleGANs shown in Fig. 1. We have tested other models and found that progressive growing GANs take a long time to learn high–quality images and have a problem finding latent vectors [26], and Variational AutoEncoder tends to generate blurry images [27].

It is widely known that training deep learning algorithms requires a sufficient amount of data. However, it is difficult to obtain medical imaging data because there are few pathologically positive cases, and are closely related to privacy issues. The GANs are widely used in medical image synthesis because they can overcome these problems [28].

Zhang et al. [29] synthesized images using GANs to perform thyroid tissue recognition. As a result of measuring the performance of the CNN model using the generated images, it was possible to solve the problem of insufficient medical image samples by demonstrating that overall classification performance was improved. Similarly, Shin et al. [30] introduced the synthesis of brain tumor MRI using GANs. The generated images were used to perform segmentation, and as a result, performance could be improved compared to the case where it was not used.

In addition, a number of researchers have attempted to use GANs in medical imaging in various applications as well as image synthesis. In this field, The GANs are also utilized for detecting abnormal images [31], segmentation [32], and others [33], [34].

In medical imaging applications, there are various motivations for using GANs, but in most cases, the main purposes were to secure the training data of the model using plausible generated data. On the other hand, there is a difference in that our purpose is to generate disease progression to aid with clinical algorithms.

A number of researchers have also attempted to detect pneumonia using deep learning. Rajpurkar et al. [4] proposed CheXNet with 121 convolutional neural networks (CNN) layers. CheXNet used the ChestX–ray14 dataset [35] for 14 disease classifications and showed 76.8% accuracy for pneumonia. Saul et al. [6] achieved 78.73% accuracy in early diagnosis of pneumonia using a simpler CNN structure than previously mentioned.

In some works, authors diagnosed pneumonia by transfer learning to use a pre–trained network structure such as Xception [36], VGG [37], or ResNet [38]. These works performed an accuracy of 82% for the Xception model, 87% for the VGG16 model [39], and 94.06% for the ResNet50 model [40] on Chest X–Ray Image dataset [41]. In particular, ResNet152-based architecture achieves an accuracy of 99.22% [42]. Although there are various approaches for diagnosing pneumonia, we used a ResNet152 that showed good classification performance.

ResNet [38] is a neural network architecture developed to address the issues of gradient vanishing and exploding that occur as neural networks become deeper. These problems can arise during the backpropagation in deep neural networks,

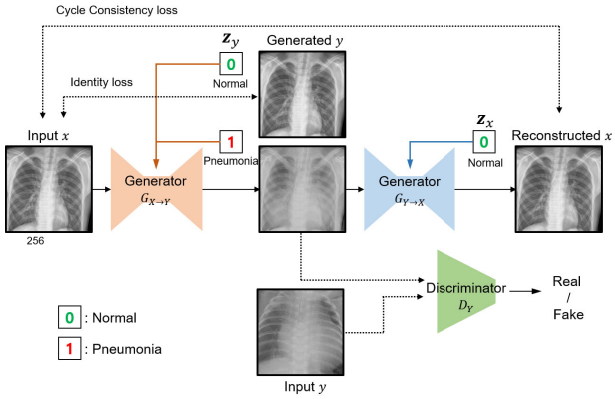

FIGURE 2. The architecture of conditional CycleGANs.

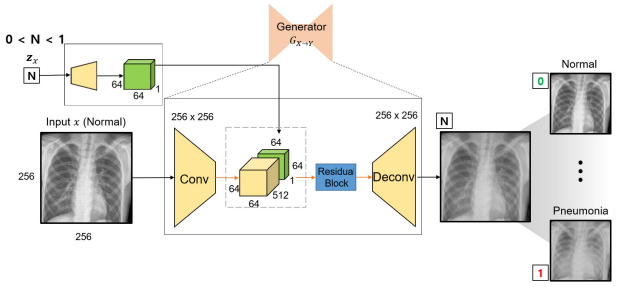

FIGURE 3. Generator structure for generating pneumonia progression.

leading to training instability and performance degradation. ResNet employs a mechanism of adding residuals to the input to obtain the output, rather than following a traditional sequential connection of layers between input and output. This approach allows the network to tackle the gradient vanishing problem in deep networks, making training more manageable. For our specific tasks, the ResNet architecture was used as a classifier by only modifying the last fully connected layer.

III. METHODOLOGY

A. ARCHITECTURE OF CONDITIONAL CycleGANs

We trained conditional CycleGANs to generate an image of the progression of pneumonia. This architecture is a conditional extension of the CycleGANs that allows the image domains to be converted according to the conditional vector received as an input.

To incorporate conditional vectors into a mapping function, we insist that there should be cycle consistency and identity according to the conditional vector. In Figure 2, conditional Cycle Consistency means that each image x from the *normal* domain X can be reverted to the original image when successively fed into the generators. Through conditional vector control, performing two complete domain translations should result in output images that are similar to the original images. In other words, it should be guaranteed that $G_{Y\to X}(G_{X\to Y}(x|c_1)|c_0) \approx x$, where c_0 is the conditional input for the normal image, c_1 is the conditional input for the pneumonia image. We derive these properties through the conditional Cycle Consistency loss defined as:

$$\mathcal{L}_{\text{cCYC}}(G_{X\to Y}, G_{Y\to X}) = \| G_{Y\to X}(G_{X\to Y}(x|c_1)|c_0) - x \|_1 + \| G_{X\to Y}(G_{Y\to X}(y|c_0)|c_1) - y \|_1 \quad (5)$$

Additionally, we introduce Identity loss for fusing conditional information into the generators. Reverting each image x from the *normal* domain X to the original image when fed into the generator with normal conditional vector c_0, and it should be able to guarantee $G_{X\to Y}(x|c_0) \approx x$. We encourage this behavior through Identity loss defined as:

$$\mathcal{L}_{\text{cID}}(G_{X\to Y}, G_{Y\to X}) = \| G_{X\to Y}(x|c_0) - x \|_1 + \| G_{Y\to X}(y|c_1) - y \|_1 \quad (6)$$

The full loss function of the GANs we proposed is as follows:

$$\begin{aligned}\mathcal{L}(G_{X\to Y}, G_{Y\to X}, D_X, D_Y) = {} & \mathcal{L}_{\text{cGANs}}(G_{X\to Y}, D_Y) \\ & + \mathcal{L}_{\text{cGANs}}(G_{Y\to X}, D_X) \\ & + \lambda_1 \mathcal{L}_{\text{cCYC}}(G_{X\to Y}, G_{Y\to X}) \\ & + \lambda_2 \mathcal{L}_{\text{cID}}(G_{X\to Y}, G_{Y\to X}) \quad (7)\end{aligned}$$

where λ_1, and λ_2 are the hyper–parameters that control the weight of the conditional Cycle Consistency and Identity loss, respectively.

The architecture for changing the normal images to the pneumonia images is shown in Fig. 2 where domain X is the space of normal images and domain Y is the space of pneumonia images. As mentioned in Section II, The goal of CycleGANs is to use the training dataset to change a domain X image to domain Y or vice versa.

B. TRAINING PROCESS AND EVALUATION

In order to train the proposed GANs structure, we first generated a fake image by using an image with a conditional vector corresponding to each domain as an input of generators. The conditional vector corresponding to the desired class is input to the generator. Therefore, one generator can synthesize images for several classes according to the conditional vector. For example, the generator $G_{X\to Y}$ can synthesize an image $G_{X\to Y}(x|c_1)$ belongs to class *pneumonia* and an image $G_{X\to Y}(x|c_0)$ for class *normal*.

Subsequently, based on the original image and the generated image, the Cycle Consistency and Identity loss can be calculated as demonstrated in Eq. (4, 6), and the final loss of the proposed model can be obtained as shown in Eq. (7). The generators and discriminators are updated based on the calculated loss. The procedures of training conditional CycleGANs are summarized in Algorithm 1.

Fig. 2 shows that we input 0 or 1 as a conditional vector to train conditional CycleGANs. After training GANs, in order to generate images showing the progression of pneumonia,

Algorithm 1 Algorithm for Conditional CycleGANs Training

Input: The conditional vector c based on disease;
The images x,y according each domain X, Y;
Hyper–parameters $\lambda_1 = 10$ and $\lambda_2 = 5$;
Output: Trained conditional CycleGANs structure

for number of epochs N **do**
  for number of epochs N **do**
    Generate m samples of $G_{X\to Y}(x|c_1)$
    Generate m samples of $G_{Y\to X}(y|c_0)$
    Calculate Identity loss $\|G_{X\to Y}(x|c_0) - x\|_1$
    Calculate Identity loss $\|G_{Y\to X}(y|c_1) - y\|_1$
    Calculate Cycle loss $\|G_{Y\to X}(G_{X\to Y}|c_1)|c_0) - x\|_1$
    Calculate Cycle loss $\|G_{X\to Y}(G_{Y\to X}|c_0)|c_1) - y\|_1$
    update the Generators $G_{X\to Y}$ and $G_{Y\to X}$
    $\min_G \mathcal{L}(G_{X\to Y}, G_{Y\to X}, D_X, D_Y)$
    update the Discriminators D_X and D_Y
    $\max_D \mathcal{L}_{\text{cGANs}}(G, D)$
  end for
end for
return Trained networks $G_{X\to Y}$, $G_{Y\to X}$ and D_X, D_Y

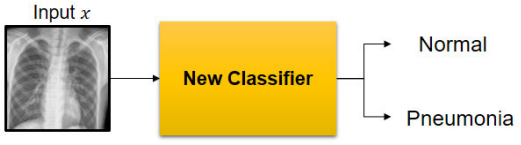

(a) Classification for test images

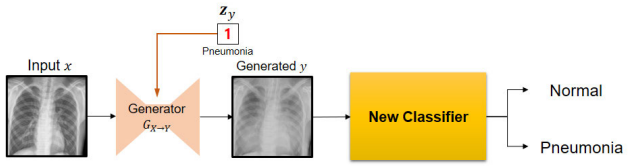

(b) Classification for domain changed test images

FIGURE 4. ResNet based classification for the test image.

we gave a real number between 0 and 1 as the input of the conditional vector, as shown in Fig. 3.

After training of the proposed model is completed, we used a pre–trained ResNet152 [38] to determine if the images generated by CycleGANs were plausible. We redefined the end point of pre–trained ResNet152 as a new classifier so that pneumonia images and normal images could be classified. Then, to verify the CycleGANs learning, we used the new classifier with test images and domain–changed test images.

IV. EXPERIMENTS AND DISCUSSION

A. DATASET

In this study, the dataset we used to generate the progression of pneumonia was the CXR Image dataset collected and labeled by Kermany et al. [41]. This dataset consists of 5,856 CXR images and has two categories, normal and pneumonia. Table. 1 shows the distribution by dataset categories.

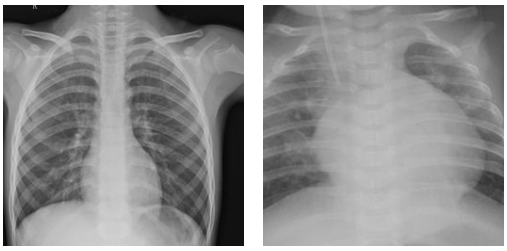

(a) Normal (b) Pneumonia

FIGURE 5. Example images from the Chest X–Ray Image dataset.

TABLE 1. The distribution of dataset.

	Train	Validation	Test
Normal	1,341	8	234
Pneumonia	3,875	8	390
Total	5,216	16	624

This dataset consists of CXR images for pediatric patients from 1 to 5 years old at Guangzhou Women and Children's Medical Center, Guangzhou. In the case of images with low quality, it was excluded through determine of three experts. We modified the image size to 256 × 256 for training GANs, and the result image is shown in Fig. 5. The pneumonia X–ray shows white spots on the bronchial area, which indicate inflammation or inflammatory exudate.

B. IMPLEMENTATION DETAILS

Our experiment can be divided into two stages. The first step is to train conditional CycleGANs, and the second step is to verify the trained GANs and then generate images of the disease progression.

To perform the first step, the generators of proposed GANs were constructed with 9 residual blocks, and the discriminators were composed of 4 Convolution layers using Leaky ReLUs with a slope of 0.2. By default, the learning rate was set to 0.0002, and Adam with parameters $\beta_1 = 0.5$, $\beta_2 = 0.999$ were used as the optimization function. To calculate the final loss, The hyper–parameters $\lambda_1 = 10$ for Cycle Consistency loss and $\lambda_2 = 5$ for Identity loss were used [24]. We used transfer learning for the following procedure. For our purposes, we fine-tuned the pre-trained model and adapted the CXR images to classify pneumonia and normal images.

C. RESULTS

Fig. 6 (a) and (b) show real and fake samples that correspond with each other after training GANs for 200 epochs. Fig. 7 and Table. 2 present classification results by dataset type. In both cases, the performance metric results were similar, with a tendency for stricter evaluation of normal images. In other words, it was more common for the classifier to judge normal images as pneumonia than for it to classify pneumonia

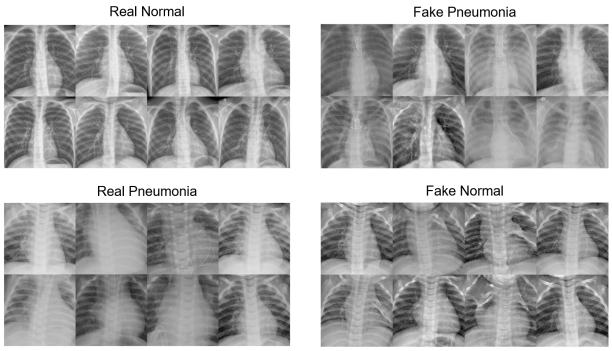

(a) Real samples (b) Fake samples

FIGURE 6. The result images of trained GANs for domain conversion. (a) : samples from real dataset. (b) : fake images that correspond to the real ones generated through CycleGANs.

TABLE 2. The classification result by dataset type.

Dataset	Domain	Classified as Normal	Classified as Pneumonia	Total
Original	Normal	136	98	234
	Pneumonia	8	382	390
Generated	Normal → Pneumonia	7	227	234
	Pneumonia → Normal	299	91	390

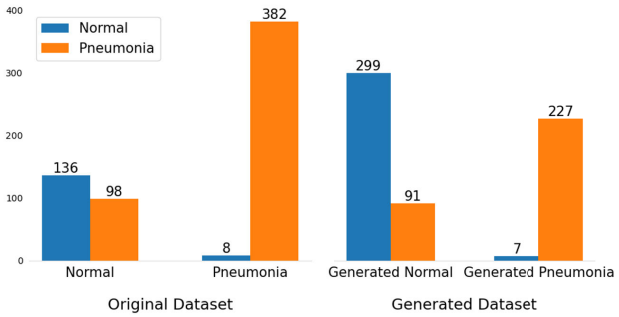

FIGURE 7. Bar plot of the confusion matrix by dataset type.

images as normal. The classification of test images using the new classifier showed 79.6% precision, 97.9% recall, and 87.8% F1–score. For generated test images that changed domain, the classification showed 71.4 % precision, 97 % recall, and 82.3 % F1–score.

Fig. 8 displays some sample images. It shows the converted image from the real image on the left to the fake image on the right. Through the training process of the GANs, the characteristics of pneumonia can be well captured and see that it was naturally converted to each domain.

Fig. 9 presents the classification probabilities of the original and generated dataset, which is the output value obtained by inputting the image of each dataset into the new classifier. Fig. 9 (a) shows the probability that a normal image is classified as a pneumonia image, and the probability distributions for both original and generated images are spread widely from 0 to 1, showing similar distributions. In the case of fake images, the figure shows that the

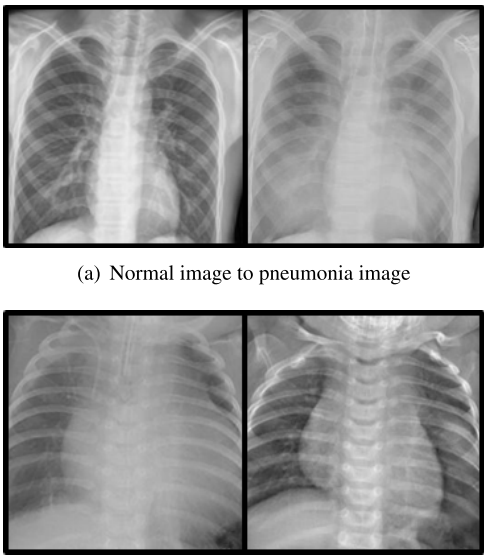

(a) Normal image to pneumonia image

(b) Pneumonia image to normal image

FIGURE 8. Sample conversion result images.

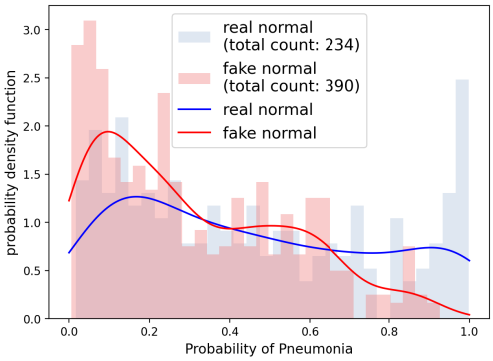

(a) The probability of classifying normal as pneumonia.

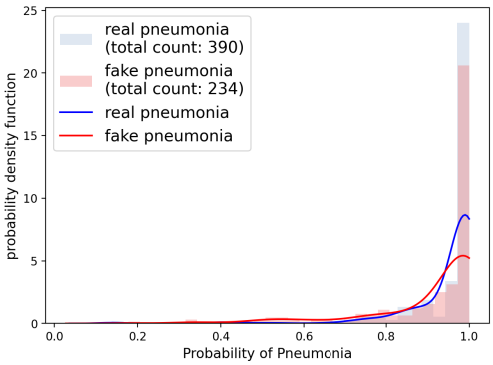

(b) The probability of classifying pneumonia as pneumonia

FIGURE 9. Comparison of probability distributions between original and generated dataset.

closer the probability of determining pneumonia is to 1, the more pronounced the decrease in probability density, which confirms that the GANs were well–trained. The probability that a pneumonia image as a pneumonia image is shown

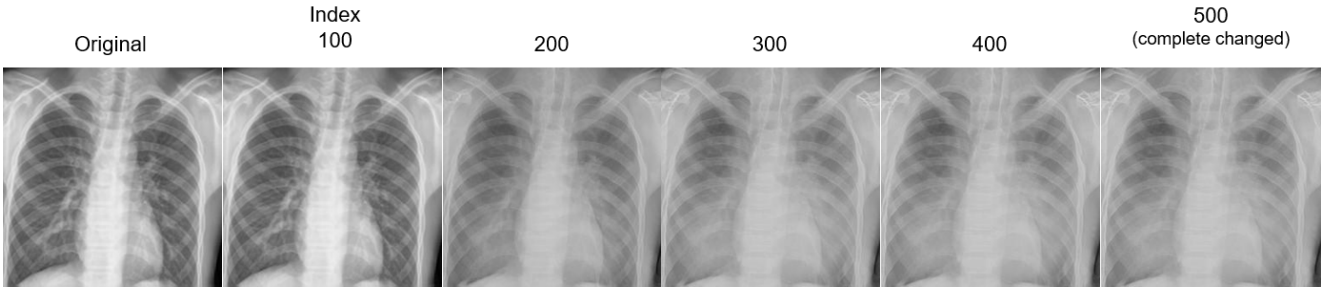

(a) The progression process from normal to pneumonia

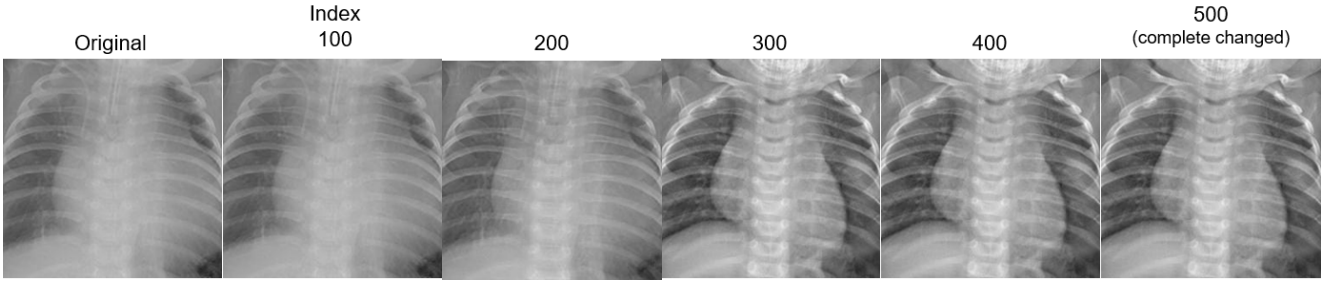

(b) The progression process from pneumonia to normal

FIGURE 10. **The generated results of image progression according to conditional input values.**

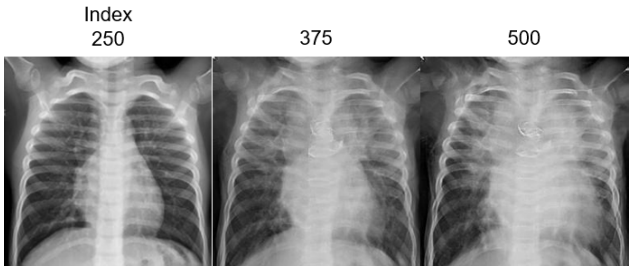

(a) Images according to index.

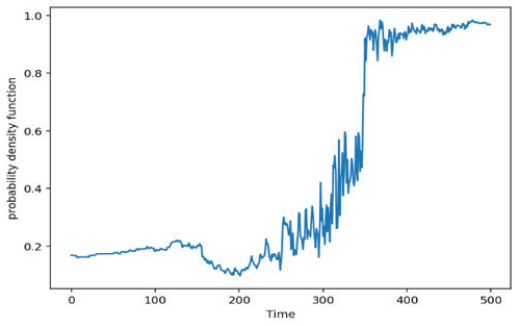

(b) Probability of diagnosing pneumonia according to index.

FIGURE 11. **Probability of diagnosing pneumonia as index progresses.**

in Fig. 9 (b), and unlike in Fig. 9 (a), the classification is more stringent. In addition, both the real and the fake images show a concentrated probability distribution when pneumonia probability is close to 1.

To obtain lapsed pneumonia images, we applied 500 real numbers at equal intervals between 0 and 1 to Eq (8) and then input each as a conditional vector in the trained generator. Where the default of *base* is 50,000 and x is used a value that increases by 0.002 between 0 and 1.

$$\text{conditionalvector} = \frac{base^x - 1}{base - 1} \tag{8}$$

The image that generated the progression of pneumonia is shown in Fig. 10. This image was the result of entering the value of the conditional vector corresponding to each index between 0 and 1, and it seems that the domain changed well in the images. there is a point that changes dramatically in the middle. We extracted the intermediate image changing from the normal image to the pneumonia image, and the graph shows the probability of diagnosing pneumonia according to each index change using our classifier. There is a rapid change between the 300th and 400th indexes, and in addition, in the process of generating a progression of pneumonia, we found not only spreading exudate but also enlarged hearts in Fig. 11. This finding presented the possibility our applying our method to expressing this change process as well. We also expect that research on a clinical pneumonia algorithm will be possible through analysis before and after the point where a classifier considers pneumonia.

However, although the value was converted according to each index as in Eq (8) to capture the smooth change, there are several limitations. It is not changing at a constant rate between the two latent vectors. As shown in the graph in Fig. 11 (b), the closer the end point, the faster the change can be observed, and this suggests the need for further study of the latent space. Moreover, the pneumonia images labeled by medical experts were used, and other

chest conditions were not considered. Since the classifier was used for performance evaluation of the generated data, no explanations were provided for disease diagnosis. Finally, with the stable learning ability of CycleGANs, it is possible to generate higher resolution images than the image resolution used in common research, but the resolution is still lower than that in actual X–ray images.

V. CONCLUSION

We used conditional CycleGANs to generate images of the progression of pneumonia by inputting 0 and 1 as conditional vectors, and we evaluated its performance with the newly defined classifier based on ResNet152. Through our results, we confirmed that the conditional CycleGANs were able to generate fake normal and fake pneumonia x-ray images that look like real images. Then, we used the generator of the trained GANs to create the progression of the disease by giving the real number between 0 and 1 to the input value of the conditional vector.

Analyzing the generated images confirmed that the exudate of pneumonia spreads to whole areas and the heart is enlarged. Based on these findings, we propose the possibility of applying these trained GANs to express other change processes. In addition, in the probability of diagnosing pneumonia on the X–ray image, we detected a rapid change in probability in certain areas, which confirmed the possibility of studying the clinical algorithms of pneumonia on X–ray images.

In future works, we would like to simultaneously or independently generate the progression of diseases in addition to pneumonia by increasing the dimension of the conditional vector and also study using X–ray images as part of a diagnostic method through the detection of probability changes.

REFERENCES

[1] O. Ruuskanen, E. Lahti, L. C. Jennings, and D. R. Murdoch, "Viral pneumonia," *Lancet*, vol. 377, no. 9773, pp. 1264–1275, 2011.

[2] K. K. Yadav and S. Awasthi, "The current status of community-acquired pneumonia management and prevention in children under 5 years of age in India: A review," *Therapeutic Adv. Infectious Disease*, vol. 3, nos. 3–4, pp. 83–97, Jun. 2016.

[3] Y. Esayag, I. Nikitin, J. Bar-Ziv, R. Cytter, I. Hadas-Halpern, T. Zalut, and A. M. Yinnon, "Diagnostic value of chest radiographs in bedridden patients suspected of having pneumonia," *Amer. J. Med.*, vol. 123, no. 1, pp. 88.e1–88.e5, Jan. 2010.

[4] P. Rajpurkar, J. Irvin, K. Zhu, B. Yang, H. Mehta, T. Duan, D. Ding, A. Bagul, C. Langlotz, K. Shpanskaya, M. P. Lungren, and A. Y. Ng, "CheXNet: Radiologist-level pneumonia detection on chest X-rays with deep learning," 2017, *arXiv:1711.05225*.

[5] H. Salehinejad, S. Valaee, T. Dowdell, E. Colak, and J. Barfett, "Generalization of deep neural networks for chest pathology classification in X-rays using generative adversarial networks," in *Proc. IEEE Int. Conf. Acoust., Speech Signal Process. (ICASSP)*, Apr. 2018, pp. 990–994.

[6] C. Jozef Saul, D. Y. Urey, and C. D. Taktakoglu, "Early diagnosis of pneumonia with deep learning," 2019, *arXiv:1904.00937*.

[7] T. Malygina, E. Ericheva, and I. Drokin, "GANs' N lungs: Improving pneumonia prediction," 2019, *arXiv:1908.00433*.

[8] B. Bozorgtabar, D. Mahapatra, H. von Tengg-Kobligk, A. Poellinger, L. Ebner, J.-P. Thiran, and M. Reyes, "Informative sample generation using class aware generative adversarial networks for classification of chest xrays," *Comput. Vis. Image Understand.*, vol. 184, pp. 57–65, Jul. 2019.

[9] A. Krizhevsky, I. Sutskever, and G. E. Hinton, "ImageNet classification with deep convolutional neural networks," in *Proc. Adv. Neural Inf. Process. Syst.*, 2012, pp. 1097–1105.

[10] A. Karpathy and L. Fei-Fei, "Deep visual-semantic alignments for generating image descriptions," in *Proc. IEEE Conf. Comput. Vis. Pattern Recognit. (CVPR)*, Jun. 2015, pp. 3128–3137.

[11] R. Dahl, M. Norouzi, and J. Shlens, "Pixel recursive super resolution," in *Proc. IEEE Int. Conf. Comput. Vis. (ICCV)*, Oct. 2017, pp. 5449–5458.

[12] L. Deng, J. Li, J.-T. Huang, K. Yao, D. Yu, F. Seide, M. Seltzer, G. Zweig, X. He, J. Williams, Y. Gong, and A. Acero, "Recent advances in deep learning for speech research at Microsoft," in *Proc. IEEE Int. Conf. Acoust., Speech Signal Process.*, May 2013, pp. 8604–8608.

[13] T. Young, D. Hazarika, S. Poria, and E. Cambria, "Recent trends in deep learning based natural language processing," 2017, *arXiv:1708.02709*.

[14] A. M. Elkahky, Y. Song, and X. He, "A multi-view deep learning approach for cross domain user modeling in recommendation systems," in *Proc. 24th Int. Conf. World Wide Web*, May 2015, pp. 278–288.

[15] X. Feng, H. Zhang, Y. Ren, P. Shang, Y. Zhu, Y. Liang, R. Guan, and D. Xu, "The deep learning–based recommender system 'pubmender' for choosing a biomedical publication venue: Development and validation study," *J. Med. Internet Res.*, vol. 21, no. 5, May 2019, Art. no. e12957.

[16] D. Ravì, C. Wong, F. Deligianni, M. Berthelot, J. Andreu-Perez, B. Lo, and G.-Z. Yang, "Deep learning for health informatics," *IEEE J. Biomed. Health Informat.*, vol. 21, no. 1, pp. 4–21, Jan. 2017.

[17] A. Fourcade and R. H. Khonsari, "Deep learning in medical image analysis: A third eye for doctors," *J. Stomatol., Oral Maxillofacial Surg.*, vol. 120, no. 4, pp. 279–288, Sep. 2019.

[18] Y. Cai, M. Landis, D. T. Laidley, A. Kornecki, A. Lum, and S. Li, "Multi-modal vertebrae recognition using transformed deep convolution network," *Comput. Med. Imag. Graph.*, vol. 51, pp. 11–19, Jul. 2016.

[19] N. Tajbakhsh, J. Y. Shin, S. R. Gurudu, R. T. Hurst, C. B. Kendall, M. B. Gotway, and J. Liang, "Convolutional neural networks for medical image analysis: Full training or fine tuning?" *IEEE Trans. Med. Imag.*, vol. 35, no. 5, pp. 1299–1312, May 2016.

[20] G. Litjens, T. Kooi, B. E. Bejnordi, A. A. A. Setio, F. Ciompi, M. Ghafoorian, J. A. W. M. van der Laak, B. van Ginneken, and C. I. Sánchez, "A survey on deep learning in medical image analysis," *Med. Image Anal.*, vol. 42, pp. 60–88, Dec. 2017.

[21] I. Goodfellow, J. Pouget-Abadie, M. Mirza, B. Xu, D. Warde-Farley, S. Ozair, A. Courville, and Y. Bengio, "Generative adversarial nets," in *Proc. Adv. Neural Inf. Process. Syst.*, 2014, pp. 2672–2680.

[22] T. Iqbal and H. Ali, "Generative adversarial network for medical images (MI-GAN)," 2018, *arXiv:1810.00551*.

[23] M. Frid-Adar, I. Diamant, E. Klang, M. Amitai, J. Goldberger, and H. Greenspan, "GAN-based synthetic medical image augmentation for increased CNN performance in liver lesion classification," *Neurocomputing*, vol. 321, pp. 321–331, Dec. 2018.

[24] J.-Y. Zhu, T. Park, P. Isola, and A. A. Efros, "Unpaired image-to-image translation using cycle-consistent adversarial networks," in *Proc. IEEE Int. Conf. Comput. Vis. (ICCV)*, Oct. 2017, pp. 2242–2251.

[25] M. Mirza and S. Osindero, "Conditional generative adversarial nets," 2014, *arXiv:1411.1784*.

[26] T. Karras, T. Aila, S. Laine, and J. Lehtinen, "Progressive growing of GANs for improved quality, stability, and variation," 2017, *arXiv:1710.10196*.

[27] D. P. Kingma and M. Welling, "Auto-encoding variational Bayes," 2013, *arXiv:1312.6114*.

[28] X. Yi, E. Walia, and P. Babyn, "Generative adversarial network in medical imaging: A review," *Med. Image Anal.*, vol. 58, Dec. 2019, Art. no. 101552.

[29] Q. Zhang, H. Wang, H. Lu, D. Won, and S. W. Yoon, "Medical image synthesis with generative adversarial networks for tissue recognition," in *Proc. IEEE Int. Conf. Healthcare Informat. (ICHI)*, Jun. 2018, pp. 199–207.

[30] H.-C. Shin, N. A. Tenenholtz, J. K. Rogers, C. G. Schwarz, M. L. Senjem, J. L. Gunter, K. P. Andriole, and M. Michalski, "Medical image synthesis for data augmentation and anonymization using generative adversarial networks," in *Proc. Int. Workshop Simulation Synth. Med. Imag.* Springer, 2018, pp. 1–11.

[31] T. Schlegl, P. Seeböck, S. M. Waldstein, U. Schmidt-Erfurth, and G. Langs, "Unsupervised anomaly detection with generative adversarial networks to guide marker discovery," in *Proc. Int. Conf. Inf. Process. Med. Imag.* Springer, 2017, pp. 146–157.

[32] Y. Li and L. Shen, "CC-GAN: A robust transfer-learning framework for HEp-2 specimen image segmentation," *IEEE Access*, vol. 6, pp. 14048–14058, 2018.
[33] Q. Yang, P. Yan, Y. Zhang, H. Yu, Y. Shi, X. Mou, M. K. Kalra, Y. Zhang, L. Sun, and G. Wang, "Low-dose CT image denoising using a generative adversarial network with Wasserstein distance and perceptual loss," *IEEE Trans. Med. Imag.*, vol. 37, no. 6, pp. 1348–1357, Jun. 2018.
[34] K. Armanious, C. Jiang, S. Abdulatif, T. Küstner, S. Gatidis, and B. Yang, "Unsupervised medical image translation using cycle-MedGAN," in *Proc. 27th Eur. Signal Process. Conf. (EUSIPCO)*, Sep. 2019, pp. 1–5.
[35] X. Wang, Y. Peng, L. Lu, Z. Lu, M. Bagheri, and R. M. Summers, "ChestX-ray8: Hospital-scale chest X-ray database and benchmarks on weakly-supervised classification and localization of common thorax diseases," in *Proc. IEEE Conf. Comput. Vis. Pattern Recognit. (CVPR)*, Jul. 2017, pp. 2097–2106.
[36] F. Chollet, "Xception: Deep learning with depthwise separable convolutions," 2016, *arXiv:1610.02357*.
[37] K. Simonyan and A. Zisserman, "Very deep convolutional networks for large-scale image recognition," 2014, *arXiv:1409.1556*.
[38] K. He, X. Zhang, S. Ren, and J. Sun, "Deep residual learning for image recognition," 2015, *arXiv:1512.03385*.
[39] E. Ayan and H. M. Ünver, "Diagnosis of pneumonia from chest X-ray images using deep learning," in *Proc. Sci. Meeting Electr.-Electron. Biomed. Eng. Comput. Sci. (EBBT)*, Apr. 2019, pp. 1–5.
[40] N. Ansari, A. Faizabadi, S. Motakabber, and M. Ibrahimy, "Effective pneumonia detection using ResNet based transfer learning," *Test Eng. Manage.*, vol. 82, pp. 15146–15153, Feb. 2020.
[41] D. S. Kermany et al., "Identifying medical diagnoses and treatable diseases by image-based deep learning," *Cell*, vol. 172, no. 5, pp. 1122–1131, Feb. 2018.
[42] N. M. Elshennawy and D. M. Ibrahim, "Deep-pneumonia framework using deep learning models based on chest X-ray images," *Diagnostics*, vol. 10, no. 9, p. 649, Aug. 2020.

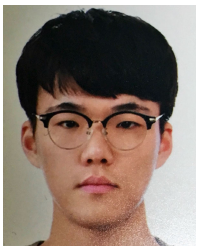

YEONGBONG JIN received the B.S. and M.S. degrees in statistics from Chonnam National University, South Korea, in 2019 and 2021, respectively. He is currently pursuing the Ph.D. degree with Seoul National University. His current research interests include machine learning algorithms, artificial intelligence methodologies, and financial time series analysis.

WOOJIN CHANG received the B.Sc. degree in fiber polymer engineering from Seoul National University, Seoul, South Korea, in 1997, and the M.Sc. degree in operations research and the Ph.D. degree in industrial engineering from the Georgia Institute of Technology, GA, USA, in 1998 and 2002, respectively. From 2002 to 2003, he was an Assistant Professor with the Department of Decision Sciences and Engineering Systems, Rensselaer Polytechnic Institute, NY, USA. He joined the Department of Industrial Engineering, Seoul National University, in 2004, where he is currently a Professor with the Financial Risk Engineering Laboratory.

BONGGYUN KO received the B.S. and M.S. degrees in mathematical science from the Korea Advanced Institute of Science and Technology, South Korea, in 2013, and the Ph.D. degree in industrial engineering from Seoul National University, South Korea, in 2016.

From 2016 to 2018, he was a Senior Professional with the Big Data Analytics Group of Mobile Communications Business, Samsung Electronics. He was a Senior Data Scientist with the Hana Institute of Technology (Hana TI), South Korea, in 2018. He is currently an Associate Professor with the Department of Statistics, Chonnam National University, South Korea. His current research interests include machine learning algorithms, financial time series analysis, and risk management.